Article

Cancer Cell

Epigenetic Perturbations by Arg882-Mutated DNMT3A Potentiate Aberrant Stem Cell Gene-Expression Program and Acute Leukemia Development

Graphical Abstract

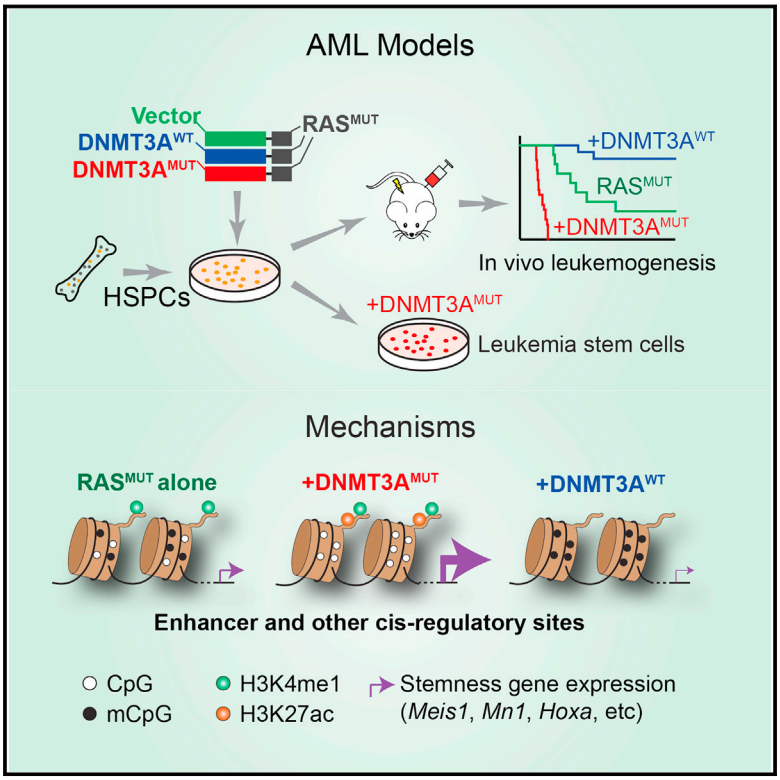

Highlights

- DNMT3A^{R882H} promotes acute leukemogenicity in the presence of mutant NRAS
- DNMT3A^{R882H} induces focal DNA hypomethylation at *cis* elements of key stemness genes
- DNMT3A^{R882H} potentiates stemness gene expression via enhancer/promoter activation
- DNMT3A^{R882H}-induced gene activation programs are sensitive to Dot1l blockade

Authors

Rui Lu, Ping Wang, Trevor Parton, ..., Paul A. Wade, Deyou Zheng, Gang Greg Wang

Correspondence

deyou.zheng@einstein.yu.edu (D.Z.), greg_wang@med.unc.edu (G.G.W.)

In Brief

Lu et al. establish that Arg882-mutated DNMT3A contributes to acute myeloid leukemia (AML) pathogenesis through epigenetic activation of leukemia-related genes. Inhibition of Dot1l reverses mutant DNMT3A-induced gene expression, indicating a potential therapeutic strategy for AMLs harboring this mutation.

Accession Numbers

GSE71475

Lu et al., 2016, Cancer Cell *30*, 92–107
July 11, 2016
http://dx.doi.org/10.1016/j.ccell.2016.05.008

CellPress

Cancer Cell
Article

Epigenetic Perturbations by Arg882-Mutated DNMT3A Potentiate Aberrant Stem Cell Gene-Expression Program and Acute Leukemia Development

Rui Lu,[1,2] Ping Wang,[3] Trevor Parton,[1] Yang Zhou,[4] Kaliopi Chrysovergis,[5] Shira Rockowitz,[6] Wei-Yi Chen,[7] Omar Abdel-Wahab,[8] Paul A. Wade,[5] Deyou Zheng,[3,6,*] and Gang Greg Wang[1,2,9,*]

[1]Lineberger Comprehensive Cancer Center
[2]Department of Biochemistry and Biophysics
University of North Carolina School of Medicine, Chapel Hill, NC 27599, USA
[3]Department of Neurology, Albert Einstein College of Medicine, Bronx, NY 10461, USA
[4]Department of Pathology and Laboratory Medicine, McAllister Heart Institute, University of North Carolina School of Medicine, Chapel Hill, NC 27599, USA
[5]Laboratory of Molecular Carcinogenesis, National Institute of Environmental Health Sciences, National Institute of Health, Research Triangle Park, NC 27709, USA
[6]Departments of Genetics and Neuroscience, Albert Einstein College of Medicine, Bronx, NY 10461, USA
[7]Institute of Biochemistry and Molecular Biology, National Yang-Ming University, Taipei 11221, Taiwan
[8]Human Oncology and Pathogenesis Program, Memorial Sloan-Kettering Cancer Center, New York, NY 10065, USA
[9]Curriculum in Genetics and Molecular Biology, University of North Carolina at Chapel Hill, Chapel Hill, NC 27599, USA
*Correspondence: deyou.zheng@einstein.yu.edu (D.Z.), greg_wang@med.unc.edu (G.G.W.)
http://dx.doi.org/10.1016/j.ccell.2016.05.008

SUMMARY

DNA methyltransferase 3A (*DNMT3A*) is frequently mutated in hematological cancers; however, the underlying oncogenic mechanism remains elusive. Here, we report that the *DNMT3A* mutational hotspot at Arg882 (*DNMT3A*^{R882H}) cooperates with *NRAS* mutation to transform hematopoietic stem/progenitor cells and induce acute leukemia development. Mechanistically, DNMT3A^{R882H} directly binds to and potentiates transactivation of stemness genes critical for leukemogenicity including *Meis1*, *Mn1*, and *Hoxa* gene cluster. DNMT3A^{R882H} induces focal epigenetic alterations, including CpG hypomethylation and concurrent gain of active histone modifications, at *cis*-regulatory elements such as enhancers to facilitate gene transcription. CRISPR/Cas9-mediated ablation of a putative *Meis1* enhancer carrying DNMT3A^{R882H}-induced DNA hypomethylation impairs *Meis1* expression. Importantly, DNMT3A^{R882H}-induced gene-expression programs can be repressed through Dot1l inhibition, providing an attractive therapeutic strategy for *DNMT3A*-mutated leukemias.

INTRODUCTION

DNA methylation provides a critical epigenetic means for defining cellular identity and regulating functional output of gene-regulatory elements such as promoters and enhancers (Jones, 2012; Schubeler, 2015). Recently, DNA methyltransferase 3A (*DNMT3A*), a de novo DNA methyltransferase gene, was found mutated in ~20%–30% of human acute myeloid leukemias (AMLs) and ~10%–20% of various other hematological cancers (Cancer Genome Atlas Research Network, 2013; Ley et al., 2010; Patel et al., 2012; Yan et al., 2011; Yang et al., 2015). *DNMT3A* mutations also associate well with clonally

Significance

Recurrent *DNMT3A* mutations at Arg882 are found in hematological malignancies and disorders; however, due to a lack of relevant disease models, molecular mechanisms by which *DNMT3A* mutations influence leukemogenesis remain largely undefined. Through establishment and characterization of murine leukemia and leukemia stem cell models, we show that *DNMT3A*^{R882H} mutation potentiates transactivation of stemness genes required for acute leukemogenicity. Integrated epigenomic profiling of murine models further reveals the underlying epigenetic alterations induced by DNMT3A^{R882H}, which are enriched at gene-regulatory sites and resemble those seen in human patients. Pharmacological inhibition of Dot1l suppresses DNMT3A^{R882H}-associated gene activation and acute leukemogenesis. Our findings not only promote mechanistic understandings of *DNMT3A* mutation-associated clonal and malignant hematopoiesis but also provide a therapeutic avenue for *DNMT3A*-mutated leukemias.

derived hematopoiesis at premalignant stages (Genovese et al., 2014; Jaiswal et al., 2014; Shlush et al., 2014; Xie et al., 2014) and often coexist with a secondary lesion that "hits" either the FLT3-RAS kinase pathway, an epigenetic regulator (*IDH1/2*, *TET2*), or *NPM1* in AML patients (Cancer Genome Atlas Research Network, 2013; Ley et al., 2010; Patel et al., 2012; Yang et al., 2015). These clinical findings suggest that *DNMT3A* mutation acts as a founder lesion and requires an additional genetic event to induce malignant development. Consistently, mice with *Dnmt3a* knockout in the bone marrow produced phenotypically normal hematopoietic stem cells (HSCs); only after rounds of transplantation did *Dnmt3a*-null HSCs display self-renewal advantages (Challen et al., 2012). Mice with *Dnmt3a* mutation alone did not develop frank AML but showed increased susceptibility to malignant development upon acquisition of additional mutations (Celik et al., 2015; Chang et al., 2015; Mayle et al., 2015; Xu et al., 2014).

Mutational hotspot at Arg882 (R882), a residue located within the homodimerization interface of DNMT3A, accounts for the majority (~60%) of *DNMT3A* mutations found in AMLs (Ley et al., 2010; Yang et al., 2015). Due to a primarily heterozygous nature of *DNMT3A* R882 mutation, it was thought to act in a dominant-negative and/or haploinsufficient manner (Holz-Schietinger et al., 2012; Kim et al., 2013; Russler-Germain et al., 2014). Clinical evidence supports this notion, as AML patients with *DNMT3A* R882 mutation exhibited focal DNA hypomethylation (Russler-Germain et al., 2014). Despite these advances, there is a lack of relevant AML animal models for studying *DNMT3A* R882 mutation. Molecular pathways and mechanisms by which *DNMT3A* mutation contributes to AML pathogenesis remain undefined. Targeted approaches for the treatment of *DNMT3A*-mutated AMLs remain to be developed.

RESULTS

DNMT3A Hotspot Mutation Enhances Sensitivity of Hematopoietic Stem/Progenitor Cells to Transformation In Vitro

Previous reports indicate that hotspot mutations of *DNMT3A* such as *DNMT3A*^{R882H} act in a dominant-negative manner by disrupting formation of a DNMT3A-associated tetramer complex required for efficient DNA methylation (Holz-Schietinger et al., 2012; Kim et al., 2013; Russler-Germain et al., 2014). These studies prompted us to ask whether ectopic expression of human DNMT3A^{R882H} in murine hematopoietic stem/progenitor cells (HSPCs) could establish a transformation phenotype in a colony-forming unit (CFU) and replating assay (Figure S1A). Initially, we found a lack of CFU-promoting effect by DNMT3A^{R882H} alone (Figures 1A–1C). We then asked whether DNMT3A^{R882H} could enhance sensitivity of HSPCs to transformation in the presence of a second oncogenic lesion. Toward this end, we used a bicistronic retroviral system to coexpress either wild-type (WT) or R882H-mutant (RH) DNMT3A, together with other mutations known to coexist with *DNMT3A* mutation in human AMLs: NRAS (NRAS^{G12D}), NPM1 (NPM1c), or IDH1 (IDH1^{R132H}) (Figure S1A) (Ley et al., 2010; Patel et al., 2012; Shih et al., 2012). Following viral transduction and drug selection, we obtained highly pure HSPCs with comparable levels of oncogene expression for CFU assays (Figures 1C, S1B, and S1C). We did not observe a CFU-promoting effect of DNMT3A^{R882H} in the presence of NPM1c or IDH1^{R132H} (Figure S1D). However, a significant increase in CFUs was seen after replating of HSPCs co-expressing DNMT3A^{R882H} and NRAS^{G12D} (hereafter referred to as "RH-RAS"), relative to those with either oncogene alone (Figures 1A and 1B). In contrast to DNMT3A^{R882H}, DNMT3A^{WT} did not promote colony formation (Figures 1A and 1B). Post replating, HSPCs expressing NRAS^{G12D} alone produced tiny and diffuse colonies of differentiated cells whereas those with RH-RAS gave rise to large, compact colonies that mainly comprised undifferentiated progenitors (Figures 1A [inset], 1B, S1E, and S1F). Importantly, cells expressing RH-RAS as derived from serially replated colonies were able to propagate and maintain their immature progenitor status in long-term liquid culture (Figures 1D and S1G), suggesting acquisition of indefinite self-renewal capability by these cells. These data have shown that, in contrast to DNMT3A^{WT}, R882-mutated DNMT3A promotes aberrant self-renewal of HSPCs and enhances their sensitivity to transformation in vitro. In addition, *NRAS*^{G12D} genetic background provides a useful platform for dissecting the role of *DNMT3A* mutation in AML development.

DNMT3A^{R882H} Acts in Concert with Activated RAS to Induce Murine AMLs In Vivo

The observed in vitro effect of DNMT3A^{R882H} on aberrant HSPC self-renewal and immortalization indicates that it could cooperate with NRAS^{G12D} to cause malignant transformation in vivo. Thus, we transplanted murine HSPCs freshly transduced with DNMT3A (either WT or RH) and/or NRAS^{G12D} to syngeneic mice. NRAS^{G12D} alone induced a myeloproliferative disease with incomplete penetrance (Figures 1E and S1H). DNMT3A^{R882H} alone did not cause detectable diseases over a 12-month monitoring period; however, in the presence of NRAS^{G12D}, it significantly accelerated development of leukemia with a shorter latency phenotype and full penetrance (Figure 1E). RH-RAS-induced leukemia was also characterized by hepatosplenomegaly (Figures 1F, 1G, and S1I), leukemic infiltration to bone marrow, spleen, and liver (Figures 1H and S1J), and elevated counts of peripheral white blood cells and blasts (Figures 1I and S1K–S1O; Table S1). Leukemia induced by RH-RAS expressed virally transduced genes at a level comparable with progenitors immortalized by RH-RAS in vitro (Figure 1J) and displayed an immature myeloid (AML) immunophenotype (Mac-1^{+}/c-Kit^{low}/Cd34^{low}/Gr1^{-}/Cd3e^{-}/Cd19^{-}/Ter119^{-}; Figures 1K, S1P, and S1Q; Table S1). Whole-exome sequencing of three independent murine AMLs identified no recurrent mutation of additional genes (Figure S1R), suggesting that DNMT3A^{R882H} and NRAS^{G12D} are sufficient to drive AML development. Interestingly, unlike DNMT3A^{R882H}, DNMT3A^{WT} suppressed leukemogenesis in vivo (Figure 1E), suggesting that normal DNMT3A activities oppose AML pathogenesis.

DNMT3A Hotspot Mutation Produces Leukemia-Initiating Stem Cells Ex Vivo in the Presence of NRAS^{G12D}

To further verify the cell transformation effect of RH-RAS, we used a previously described liquid cultivation system (Wang et al., 2007, 2009) and were able to recapitulate HSPC immortalization with RH-RAS only, and not either oncogene alone or

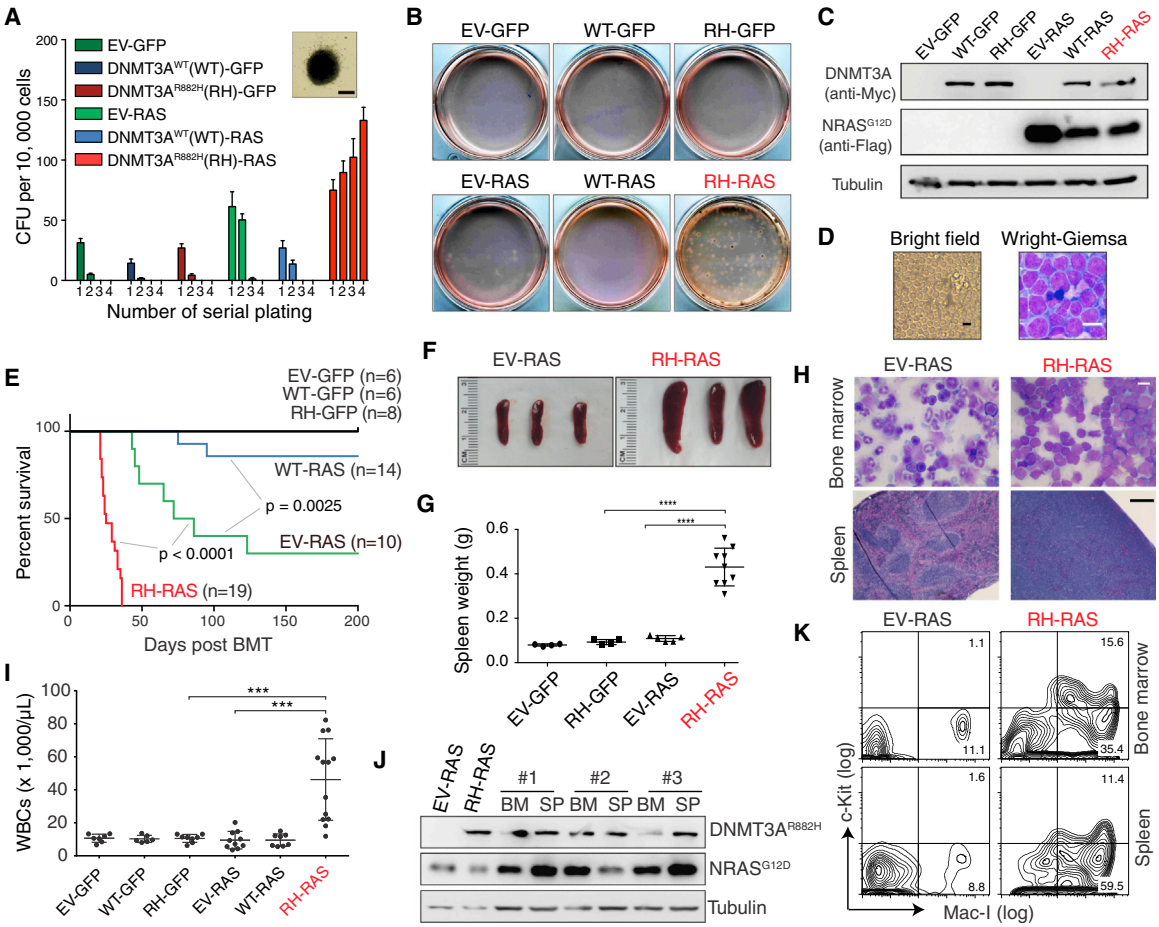

Figure 1. DNMT3A^{R882H} Acts in Concert with Mutant RAS to Transform Murine HSPCs Ex Vivo and Induce AMLs In Vivo

(A) Colony-forming unit (CFU) assay using murine HSPCs expressing empty control (EV), wild-type (WT), or R882H mutant (RH) DNMT3A in combination with GFP or NRAS^{G12D} (RAS). Inset shows a typical colony expressing RH-RAS at the fourth replating. Scale bar, 1 mm.

(B) Images of CFU assay at the fourth replating.

(C) Immunoblot of DNMT3A (Myc-tagged) and NRAS (Flag-tagged) in HSPCs after infection.

(D) Microscopic image and Wright-Giemsa staining of RH-RAS-coexpressing cells derived from the fourth replating after long-term culture with the SCF cytokine in vitro. Scale bars, 10 μm.

(E) Kaplan-Meier survival curve of mice after bone marrow transplantation (BMT) of HSPCs freshly transduced with indicated genes. The p values were calculated by log-rank test.

(F and G) Spleen size (F, n = 3) and weight (G, n = 4–9) of indicated cohorts 3–4 weeks post BMT. The p values were calculated by Student's t test.

(H) Wright-Giemsa staining of bone marrow (upper) and H&E staining of spleen (bottom) of indicated cohorts 4 weeks post BMT. Scale bar, 10 μm (upper) and 200 μm (bottom).

(I) White blood cell (WBC) counts in peripheral blood of indicated cohorts (n = 6–13) 4 weeks post BMT. The p values were calculated by Student's t test.

(J) Immunoblot of DNMT3A (Myc) and NRAS (Flag) proteins in bone marrow (BM) and spleen (SP) cells from mice with leukemia induced by RH-RAS coexpression. The first two lanes were loaded with samples of in vitro infected HSPCs.

(K) Fluorescence-activated cell sorting (FACS) analysis of Mac-1 and c-Kit with bone marrow and spleen cells of indicated cohorts 4 weeks post BMT.

Error bar denotes ±SD; ***p < 0.001, ****p < 0.0001. See also Figure S1 and Table S1.

coexpression of DNMT3A^{WT} with NRAS^{G12D} (Figure S2A). Similarly to those derived from CFU assays, RH-RAS-immortalized progenitors stably maintained their progenitor identity in vitro in the presence of SCF or Flt3 ligand, and presented with expression of immature myeloid (c-Kit^{+}/Mac-1^{low}/Gr1^{-}) and stem cell antigens (Cd34^{low}/Flt3^{+}/Sca1$^{low/-}$) as well as a lack of other lineage markers (Figures 2A, 2B, S2B, and S2C). Exposure of these progenitors to myeloid-promoting cytokines decreased cell proliferation (Figure S1G) and induced terminal myeloid differentiation (c-Kit^{-}/Mac-1^{high}/F4-80^{high}; Figures 2B and S2D), demonstrating their myeloid differentiation capability. Engraftment with each of three independent RH-RAS-immortalized progenitor lines induced murine AMLs (Figures S2E–S2H) that can be propagated in vivo with sequential transplantation (Figure 2C). Importantly, as few as 50–500 of these cells were sufficient to cause AML (Figure 2D), illustrating their leukemia-initiating stem cell (LSC) characteristic (hereafter called "LSCs$^{RH\text{-}RAS}$"). To further characterize LSCs$^{RH\text{-}RAS}$, we profiled their transcriptome and genome-wide occupancy of H3K4me1, a histone mark demarcating lineage-specific enhancers (Lara-Astiaso

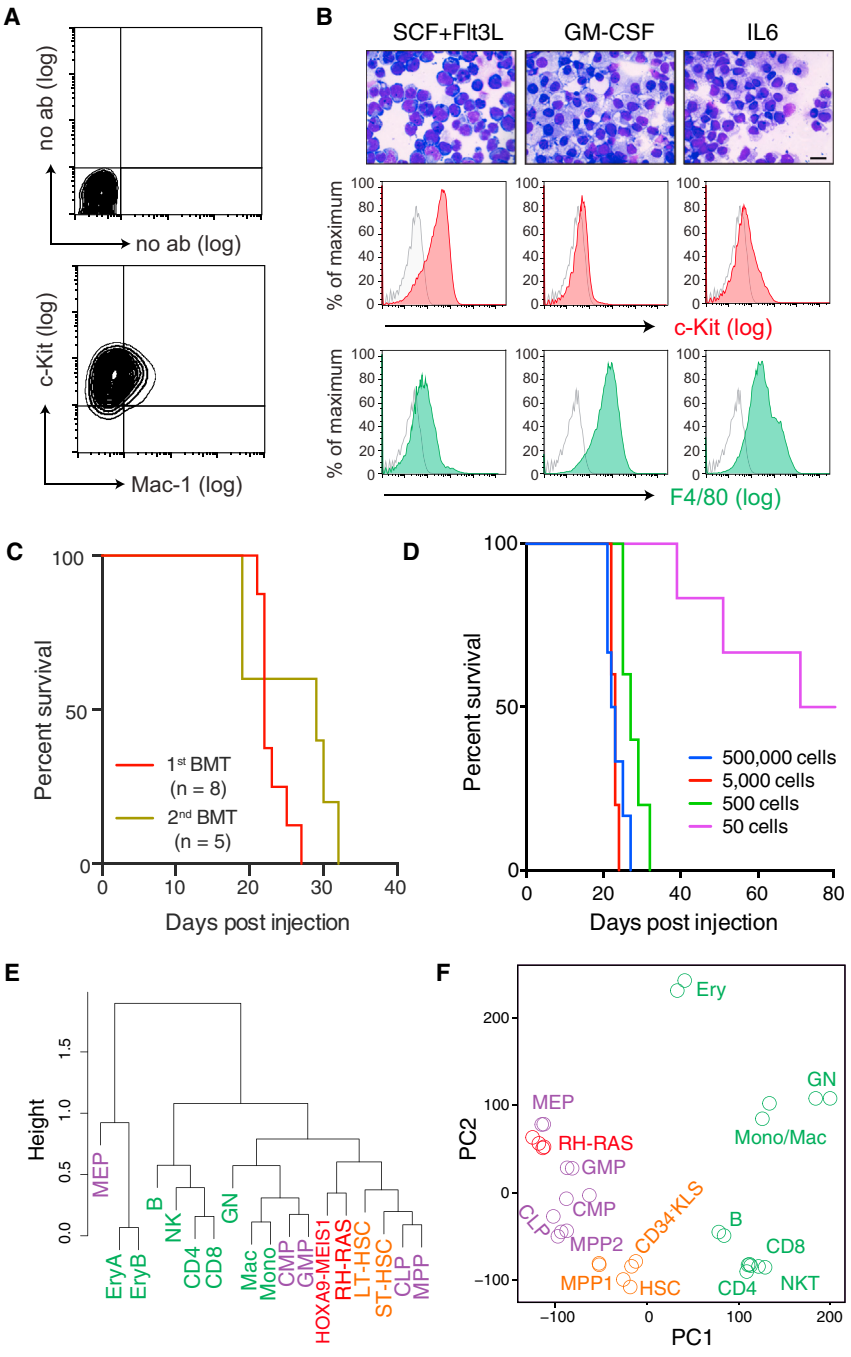

Figure 2. R882-Mutated DNMT3A Establishes Leukemia-Initiating Stem Cells Ex Vivo in the Presence of Activated RAS

(A) FACS analysis of in vitro immortalized progenitors by RH-RAS using a liquid culture system.

(B) Wright-Giemsa staining (upper) and FACS analysis of RH-RAS-immortalized progenitors 14 days after cultivation with indicated cytokines. FACS control, non-specific immunoglobulin G (gray trace). Scale bar, 10 μm.

(C) Kaplan-Meier curve of mice receiving primary or secondary BMT with RH-RAS-induced leukemia.

(D) Kaplan-Meier curve of mice (n = 5–6) receiving BMT of the indicated numbers of RH-RAS immortalized cells.

(E) Hierarchical clustering of genome-wide H3K4me1 profiles of LSCs^{RH-RAS}, AML-causing leukemia-initiating stem cell (LSC) lines produced by overexpressed HOXA9 plus MEIS1 (HOXA9-MEIS1), and various normal blood cell types. LT-HSC, long-term HSC; ST-HSC, short-term HSC; MPP, multipotent progenitor; CMP, common myeloid progenitor; CLP, common lymphoid progenitor; GMP, granulocyte-monocyte progenitor; MEP, megakaryocyte-erythroid progenitor; Mac, macrophage; Mono, monocyte; GN, granulocyte; B, B220$^+$/CD19$^+$ B cell; CD4/8, CD4/8$^+$ T cell; NK, natural killer cell; EryA and EryB, Ter119$^+$/CD71$^+$ erythroid cell with high and low forward scatter, respectively.

(F) Principal component (PC) analysis of transcriptome profiles of LSCs^{RH-RAS} and various normal blood cell types. CD34$^-$KLS, Cd34$^-$/c-Kit$^+$/Lin$^-$/Scal$^+$ HSC; MPP1, Flk2$^-$ multipotent progenitor; MPP2, Flk2$^+$ multipotent progenitor; NKT, natural killer T cell; Ery, erythroid cell. Other abbreviations as in (E).

See also Figure S2.

monality of pathways underlying leukemogenicity by these oncogenes.

R882-Mutated DNMT3A Potentiates Abnormal Transcription of Stem Cell Genes Including a Meis1-Mn1-Hoxa Regulatory Node

Next, we sought to understand the molecular basis underlying indefinite self-renewal shown by LSCs^{RH-RAS}. First, we asked whether they carry self-renewal or stemness gene-expression programs, a known feature of LSCs (Abramovich et al., 2005; et al., 2014). Unsupervised clustering of H3K4me1 profiles of LSCs^{RH-RAS} and various hematopoietic cell lineages revealed a similarity of LSCs^{RH-RAS} to HSPCs such as HSC and myeloid progenitors, when compared with differentiated cell types (Figures 2E and S2I); similar results were found in their transcriptome comparison (Figures 2F and S2J). Notably, a closer similarity was seen when comparing LSCs^{RH-RAS} with leukemic progenitors we and others previously produced using either HOXA9 plus MEIS1 (Wang et al., 2005), MLL translocation (Bernt et al., 2011), NUP98-NSD1 (Wang et al., 2007), or NUP98-JARID1A (Wang et al., 2009) (Figures 2E, S2I, and S2J), implying a common... Eppert et al., 2011; Krivtsov et al., 2006). By transcriptome analysis, we identified 54 genes uniquely expressed in LSCs^{RH-RAS} and primitive HSPCs with self-renewal capabilities, relative to differentiating and mature hematopoietic cell types (Figure 3A and Table S2). The stem cell signature genes expressed in LSCs^{RH-RAS} are only part of HSC stemness gene programs (~10%, Figure S3A); we further verified enrichment of the LSC^{RH-RAS} stemness signature in self-renewing HSCs with independent datasets (Figures S3B and S3C). The top LSC^{RH-RAS} stemness genes included *Hoxa9*, *Mn1*, *Hoxa5*, and *Meis1* (Figure 3A), which encode a set of transcription factors (TFs) and

cofactors crucial for sustaining self-renewal of normal HSCs and leukemic LSCs (Heuser et al., 2011; Huang et al., 2012; Wang et al., 2006; Wong et al., 2007). Gene targets of Meis1-Mn1-Hoxa, *Flt3* and *Sox4* (Heuser et al., 2011; Huang et al., 2012; Wang et al., 2005), were also among top stemness genes identified (Figure 3A), indicating activity of this TF regulatory circuitry in $LSCs^{RH\text{-}RAS}$. Moreover, activation of Meis1 and Hoxa in $LSCs^{RH\text{-}RAS}$ was found to be comparable with that in LSCs defined by other deregulated chromatin factors such as MLL-AF9, NUP98-JARID1A, or NUP98-NSD1, while *Mn1* and *Mycn* showed unique expression in $LSCs^{RH\text{-}RAS}$ (Figures S3D and S3E).

As $LSCs^{RH\text{-}RAS}$ carry both *DNMT3A* and *NRAS* mutations, we next asked which stemness gene signatures are dependent on $DNMT3A^{R882H}$. We performed microarray studies using HSPCs after transduction of $NRAS^{G12D}$ alone or with coexpressed DNMT3A, either WT or R882H mutant (hereafter referred to as EV-RAS, WT-RAS, or RH-RAS). These HSPCs were collected 12 and 16 days after viral transduction when their proliferation rates were comparable (Figure S2A). Among the 54 $LSC^{RH\text{-}RAS}$ stemness genes, nine were found to be upregulated by $DNMT3A^{R882H}$ at both time points, including *Meis1*, *Mn1*, and *Hoxa* (Figures 3B and S3F). Consistently, gene set enrichment analysis (GSEA) found that gene sets associated with AML development, undifferentiated myeloid cells, and NUP98-HOXA9 targets were significantly enriched in HSPCs with RH-RAS (Figure 3C). Conversely, gene sets associated with myeloid differentiation showed reduced expression in HSPCs expressing RH-RAS, relative to EV-RAS (Figure 3D), whereas the same gene sets showed enhanced expression in HSPCs expressing WT-RAS (Figure 3D), thus suggesting opposite effects of WT and R882-mutated DNMT3A on regulating genes crucial for HSPC self-renewal versus differentiation. We verified unique upregulation of *Meis1*, *Hoxa*, and *Mn1* in RH-RAS HSPCs (Figures 3E and S3G) and their induced AMLs (Figures 3F, 3G, and S3H). To functionally assess whether the activated Meis1-Mn1-Hoxa circuitry is essential for RH-RAS-induced AML development, we introduced independent small hairpin RNAs (shRNAs) of *Meis1* or *Mn1* into $LSCs^{RH\text{-}RAS}$ (Figure 3H) and found that knocking down either gene significantly impaired in vitro growth of $LSCs^{RH\text{-}RAS}$ (Figures 3I and S3I) as well as their in vivo leukemogenic function (Figures 3J, S3J, and S3K).

Together, these data reveal a role of R882-mutated *DNMT3A* in potentiating abnormal activation of stemness genes such as *Meis1*, *Mn1*, and *Hoxa*, which are required for mutant DNMT3A-mediated AML progression.

ChIP-Seq Reveals Context-Dependent Targeting of R882-Mutated DNMT3A into the LSC Genome

The $LSC^{RH\text{-}RAS}$ cellular model described above provides an ideal system for dissecting the molecular mechanism underlying $DNMT3A^{R882H}$-mediated oncogenesis. Mutant DNMT3A proteins are exclusively nuclear (Figure S4A); thus, we first mapped their genome-wide occupancy in $LSCs^{RH\text{-}RAS}$ by chromatin immunoprecipitation sequencing (ChIP-seq) using antibodies against the Myc tag fused to $DNMT3A^{R882H}$ (Figure S1A). Myc-$DNMT3A^{R882H}$ ChIP-seq gave robust and specific signals (Figure 4A); as a negative control, Myc ChIP-seq using cells without Myc-$DNMT3A^{R882H}$ expression did not detect any peaks (Figure S4B). We identified 13,705 genomic regions with significant $DNMT3A^{R882H}$ binding (i.e., $DNMT3A^{R882H}$ peaks, Table S3) in $LSCs^{RH\text{-}RAS}$, which spread over promoter and inter- or intragenic regions (Figure S4C). $DNMT3A^{R882H}$ exhibited a broad binding pattern with an average peak size of ~17 kb (Figures S4D and 4B, with an example peak at *Lig1*). Interestingly, $DNMT3A^{R882H}$ binding was stronger at intermediately transcribed genes, relative to lowly or highly expressed genes (Figure 4A), and positively correlated to CpG dinucleotide density except at CpG islands (CGIs) where $DNMT3A^{R882H}$ has a sharp drop in overall binding (Figure 4C). $DNMT3A^{R882H}$ binding regions also showed depletion of H3K4me3 (Figure 4D), a histone modification known to suppress DNMT3A binding due to an intrinsic histone H3 "reader" activity of DNMT3A's ADD domain (Guo et al., 2015; Noh et al., 2015). Intriguingly, 76.1% of $DNMT3A^{R882H}$ peaks were found in close proximity to and significantly overlapped with peaks of H3K4me1, a histone mark demarcating enhancer elements (observed/expected = 10.2, $p < 10^{-300}$; Figure 4E), as exemplified by those identified in an intron region of *Lig1* and an intergenic region of *Vegfa* (Figures 4B [inset] and S4E [boxed areas]). Ontology analysis of $DNMT3A^{R882H}$ peaks revealed their significant enrichment at genes related to normal and malignant hematopoiesis, PML-RARα targets, and *MLL* rearrangement-associated genes (Figures 4F and S4F). Notably, key AML-promoting or stemness genes upregulated by $DNMT3A^{R882H}$ such as *Meis1*, *Mn1*, *Hoxa*, and *Mycn* were all found directly bound by $DNMT3A^{R882H}$ (Figures 4G, 4H, S4G, and S4H). Collectively, our genome-wide profiling of $DNMT3A^{R882H}$ has revealed a CpG content and "histone code"-dependent targeting of R882-mutated DNMT3A into cancer cell genomes; we have also identified a previously unappreciated overlap of $DNMT3A^{R882H}$ with putative enhancer and *cis*-regulatory sites (marked by H3K4me1) at numerous developmental genes including a Meis1-Mn1-Hoxa node.

R882-Mutated DNMT3A Induces Focal Hypomethylation of CpG Sites Enriched with Gene-Regulatory Elements

We next aimed to delineate $DNMT3A^{R882H}$-induced epigenetic perturbations during AML progression. By enhanced reduced representation bisulfite sequencing (eRRBS), we mapped global DNA methylation patterns of murine HSPCs 16 days after transduction of EV-RAS, RH-RAS, or WT-RAS. Analysis of eRRBS data, which had 11–12× coverage for 6.5 million CpGs in all samples, revealed no significant changes in global CpG methylation (Figures S5A–S5C) except a moderate change at CpG shores (Figure S5C). By pairwise comparison of CpG methylation, we identified 12,889 differentially methylated CpG sites (DMCs) in HSPCs expressing RH-RAS relative to EV-RAS, with most DMCs (80.8%) hypomethylated (Figure 5A, left; hereafter termed "$DNMT3A^{R882H}$-associated hypo-DMCs"); in contrast, DMCs associated with $DNMT3A^{WT}$ are largely hypermethylated (hyper-DMCs, 80.6%; Figure 5A, right). $DNMT3A^{R882H}$-associated hypo-DMCs were found mainly in intron, intragenic, and promoter regions, while $DNMT3A^{WT}$-induced hyper-DMCs were enriched in promoters and CGIs (Figures S5D and S5E). Importantly, $DNMT3A^{R882H}$-associated hypo-DMCs were significantly enriched at genomic regions with H3K4me1 (Figure 5B) or with $DNMT3A^{R882H}$ binding (Figures

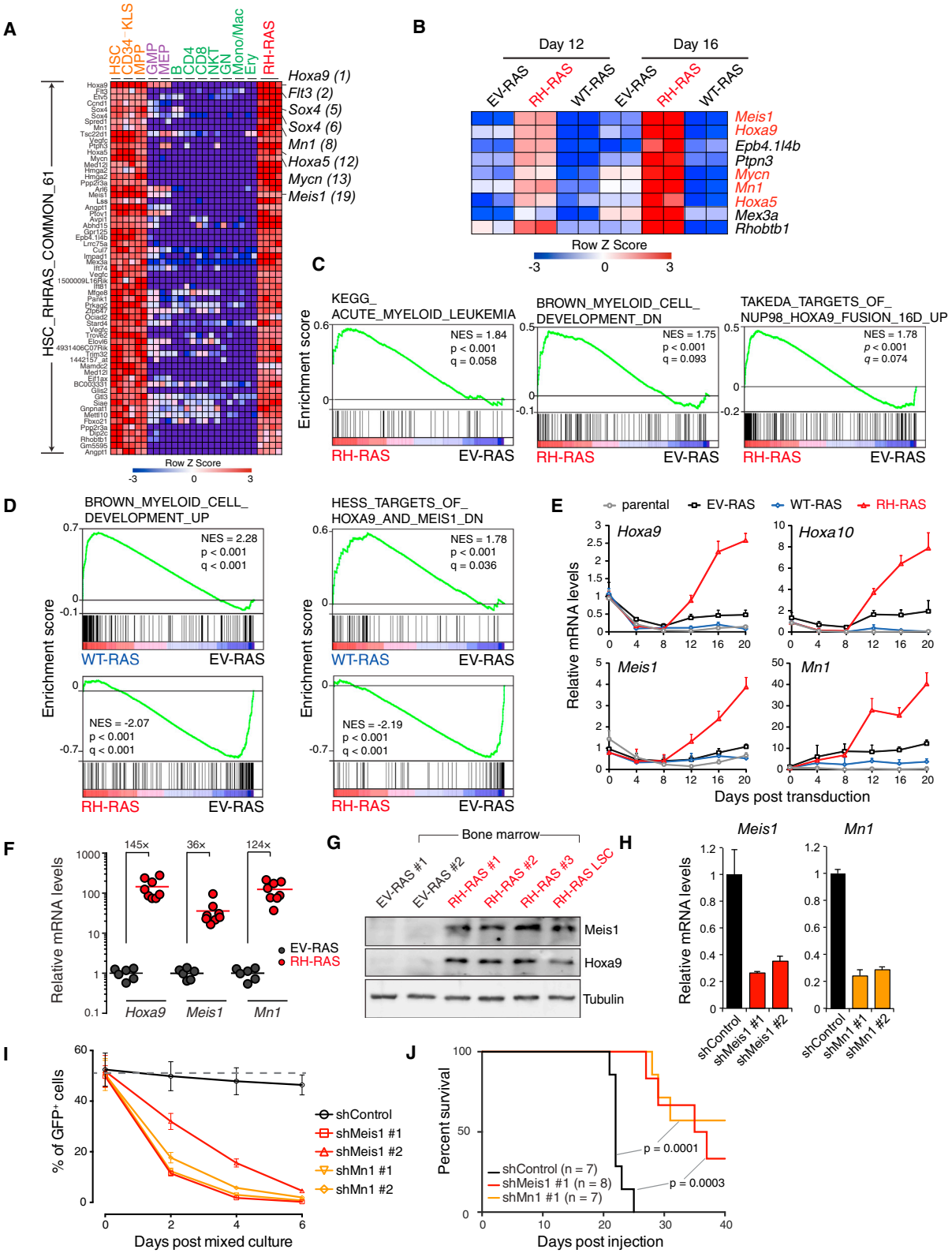

Figure 3. DNMT3A^{R882H} Potentiates Aberrant Activation of Stemness Genes Including a Critical *Meis1-Mn1-Hoxa* Regulatory Node

(A) Heatmap of 61 probes (54 genes) showing unique expression in both self-renewing HSPCs (HSC, Cd34^{-}KLS, and MPP) and LSCs^{RH-RAS} but not in differentiating (purple) or mature (green) blood cell types. Probes are ranked by higher expression in LSCs^{RH-RAS} relative to differentiating and mature cells. Example genes are highlighted along with their respective rankings.

(legend continued on next page)

5B and 5C). DNMT3A^{R882H}-associated hypo-DMCs were also found to be enriched with the binding site of the ETS family of TFs (Erg and Spi1/PU.1) and other hematopoietic TFs (Runx1 and Mycn; Figure 5D). In contrast, DNMT3A^{R882H}-associated hyper-DMCs exhibited none of these features and, instead, correlated negatively to DNMT3A^{R882H} binding (Figures 5B–5D), suggesting that creation of hyper-DMCs is due to an indirect effect of DNMT3A^{R882H}.

Consistent with DMCs, differentially methylated regions (DMRs) identified in HSPCs co-transduced with DNMT3A^{R882H} relative to control were mainly hypomethylated (hereafter called "DNMT3A^{R882H}-associated hypo-DMRs"; Table S4, n = 1,199) while DNMT3A^{WT}-associated DMRs were mainly hypermethylated (hyper-DMRs) (Figures 5E and S5F). These two sets of DMRs showed a significant overlap, including those found at DNMT3A^{R882H}-deregulated stemness genes (*Meis1*, *Mn1*, *Hoxa7*, and *Mycn*), further highlighting that WT and R882-mutated DNMT3A have opposing effects on DNA methylation of crucial AML-promoting genes (Figure 5F). In addition, DNMT3A^{R882H}-associated hypo-DMRs were enriched at genes related to transcriptional regulation, hematopoietic development, and cancer (Figures 5G and S5G). Consistent with results in DMCs, H3K4me1 and DNMT3A^{R882H} binding was significantly enriched at DNMT3A^{R882H}-associated hypo-DMRs (Figures 5H and S5H). Taken together, our results show that R882-mutated DNMT3A is sufficient to induce CpG hypomethylation at putative *cis*-regulatory sites of key stemness genes that we have functionally validated as essential for AML progression in murine models.

DNMT3A^{R882H}-Induced DNA Hypomethylation Identified in Murine Models Mirrors What Was Seen in Human AMLs with *DNMT3A* R882 Mutation

A focal CpG hypomethylation phenotype seen in the above murine model is reminiscent of what was observed in human AMLs with *DNMT3A* mutation (Russler-Germain et al., 2014). To assess whether our murine model mimics human disease, we first identified regions in the human genome that are homologous (i.e., conserved) to DNMT3A^{R882H}-associated hypo-DMRs defined in the murine model. We then found that, relative to randomized control, CpGs located in such conserved human genomic sites showed a significant reduction in their methylation levels among human AML samples with *DNMT3A* R882 mutation, relative to those with normal *DNMT3A* (Figure 5I; $p < 2.2 \times 10^{-16}$). Despite a relatively limited coverage of CpGs by the 450K-array platform used in the human AML study (Russler-Germain et al., 2014), genes with hypo-DMRs identified in AML patients carrying *DNMT3A* R882 mutation also had a significant overlap with those that gain DNMT3A^{R882H}-associated hypo-DMRs in our murine model (Table S5; $p < 0.05$). We identified 119 genes showing CpG hypomethylation in both human AMLs and murine LSC models, which again include stemness and AML-promoting genes *MEIS1*, *HOXA7*, and *MN1* (Figures 5J and S5I). We subsequently verified differential CpG methylation of DMRs at these genes in murine cells by direct bisulfite sequencing (Figures 5K and S5J), and further showed that a consistent hypomethylation pattern exists at conserved DMRs in human AMLs with *DNMT3A* R882 mutation, relative to those with non-R882 mutated or normal *DNMT3A* (Figures 5L and S5K).

Hypo-DMRs Induced by DNMT3A^{R882H} Facilitate Gain of Histone Acetylation at Gene-Regulatory Sites

Because DNMT3A^{R882H} binding and induced hypo-DMRs showed significant overlap with H3K4me1, a histone mark demarcating gene-regulatory regions such as enhancers and proximal elements close to promoters (Rada-Iglesias et al., 2011), we performed ChIP-seq profiling of H3K27ac, a histone modification correlating to enhancer/promoter activity, with the samples we used for eRRBS. Intriguingly, we found that introducing DNMT3A^{R882H} to HSPCs caused an overall gain of H3K27ac at DNMT3A^{R882H}-associated hypo-DMRs (Figure 6A, left) whereas no overall change in H3K4me1 was seen for these hypo-DMRs (Figure 6B, left); in contrast, expression of DNMT3A^{WT} decreased overall H3K27ac and H3K4me1 at these hypo-DMRs (Figures 6A and 6B, left). As a control, DNMT3A^{R882H}-associated hyper-DMRs did not show such changes (Figures 6A and 6B, right). Consistently, similar histone modification changes were seen at regions in close proximity to DNMT3A-associated DMCs (Figures S6A and S6B). Importantly, DMRs at key stemness or AML genes such as *Meis1*, *Mn1*, *Hoxa*, and *Mycn* all exhibited significant gain of H3K27ac in DNMT3A^{R882H}-expressing HSPCs as well as loss of H3K27ac in DNMT3A^{WT}-expressing HSPCs at their putative *cis*-regulatory sites (Figures 6C and S6C–S6H). By ChIP-qPCR, we verified the observed changes of H3K27ac and H3K4me1 at a panel of DMRs after transduction of DNMT3A^{R882H} versus DNMT3A^{WT} into HSPCs (Figures 6D and S6I). Furthermore, expression of DNMT3A^{R882H} enhanced binding of the H3K27 acetyltransferase p300 to hypo-DMRs at stemness genes (Figure 6E), suggesting that CpG hypomethylation facilitates recruitment of H3K27ac

(B) Of the 54 self-renewal genes, genes showing consistently higher expression in HSPCs 12 and 16 days after transduction of RH-RAS relative to EV-RAS.
(C) GSEA shows enrichment of AML-associated genes (left), genes downregulated upon myeloid differentiation (middle), and NUP98-HOXA9 targets (right) in HSPCs with RH-RAS versus EV-RAS.
(D) GSEA shows enrichment of differentiation gene sets in WT-RAS or RH-RAS HSPCs relative to EV-RAS. Left, myeloid differentiation genes; right, genes downregulated upon activation of HOXA9 and MEIS1.
(E) qRT-PCR of indicated genes in murine HSPCs after transduction of EV-RAS, WT-RAS, or RH-RAS.
(F) qRT-PCR of indicated genes in mouse bone marrow 21 days post BMT of HSPCs with EV-RAS (n = 6) or RH-RAS (n = 8).
(G) Immunoblot of Meis1 and Hoxa9 in bone marrow of mice 21 days post BMT of HSPCs with EV-RAS or RH-RAS. The last lane was loaded with LSC^{RH-RAS} samples.
(H) qRT-PCR showing shRNA-mediated *Meis1* or *Mn1* knockdown in LSCs^{RH-RAS}.
(I) Relative proliferation of indicated shRNA-expressing LSCs^{RH-RAS} (GFP$^+$) versus parental cells (GFP$^-$). These GFP$^-$ and GFP$^+$ cells were mixed in a 1:1 ratio at day 0, followed by measurement of percentage of GFP$^+$ cells.
(J) Kaplan-Meier curve of mice engrafted with indicated shRNA-expressing LSCs^{RH-RAS}. The p values were calculated by log-rank test.
Error bars denote ±SD. See also Figure S3 and Table S2.

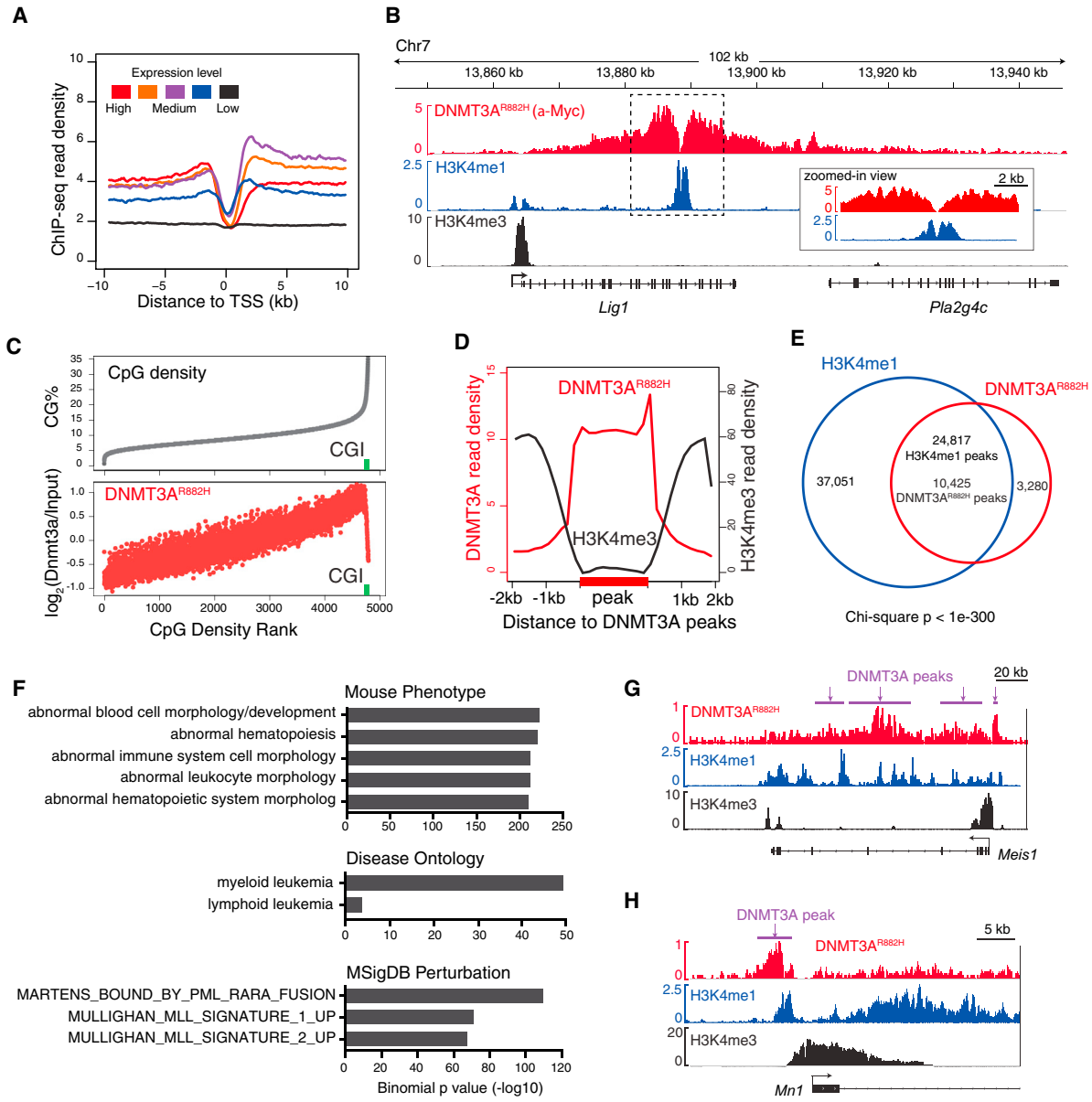

Figure 4. ChIP-Seq Reveals Chromatin Context-Dependent Binding of R882-Mutated DNMT3A to Genomic Regions, Including Stemness Genes such as a *Meis1-Mn1-Hoxa* Node

(A) DNMT3A^{R882H} ChIP-seq profiles across transcription start site (TSS) of genes with different expression levels in LSCs^{RH-RAS}.

(B) Example ChIP-seq profiles for DNMT3A^{R882H}, H3K4me1, and H3K4me3 at the Lig1 gene. Box shows a zoomed-in view of dashed-box region showing overlap of DNMT3A^{R882H} and H3K4me1 peaks.

(C) Correlation of DNMT3A^{R882H} binding and CpG density. Shown is percentage of CpG density (gray) and DNMT3A^{R882H} ChIP-seq reads (red) at 1-kb windows of the entire genome ranked by CpG density. Green square, CpG island (CGI).

(D) Plot of averaged DNMT3A^{R882H} (red) and H3K4me3 (black) ChIP-seq signals at DNMT3A^{R882H} peaks (labeled in bold on x axis) and surrounding regions (±2 kb).

(E) Venn diagram shows significant overlap of DNMT3A^{R882H} and H3K4me1 peaks in LSCs^{RH-RAS}.

(F) Genomic Regions Enrichment of Annotations Tool (GREAT) analysis shows enrichment of indicated gene signatures among DNMT3A^{R882H} peaks.

(G and H) ChIP-seq profiles of DNMT3A^{R882H}, H3K4me1 and H3K4me3 at Meis1 (G) and Mn1 (H). Purple bars, DNMT3A^{R882H} peak calls.

See also Figure S4 and Table S3.

"writers." In addition, overall gain of H3K27ac at hypo-DMRs was found to be significant regardless of expression changes of their associated genes (Figure S6J), indicating that H3K27ac gain at hypo-DMRs is not merely a consequence of gene activation, as exemplified by that found at hypo-DMRs of *Kdm2b*, *Sirt4*, and *Pax5* (Figures S6K–S6M).

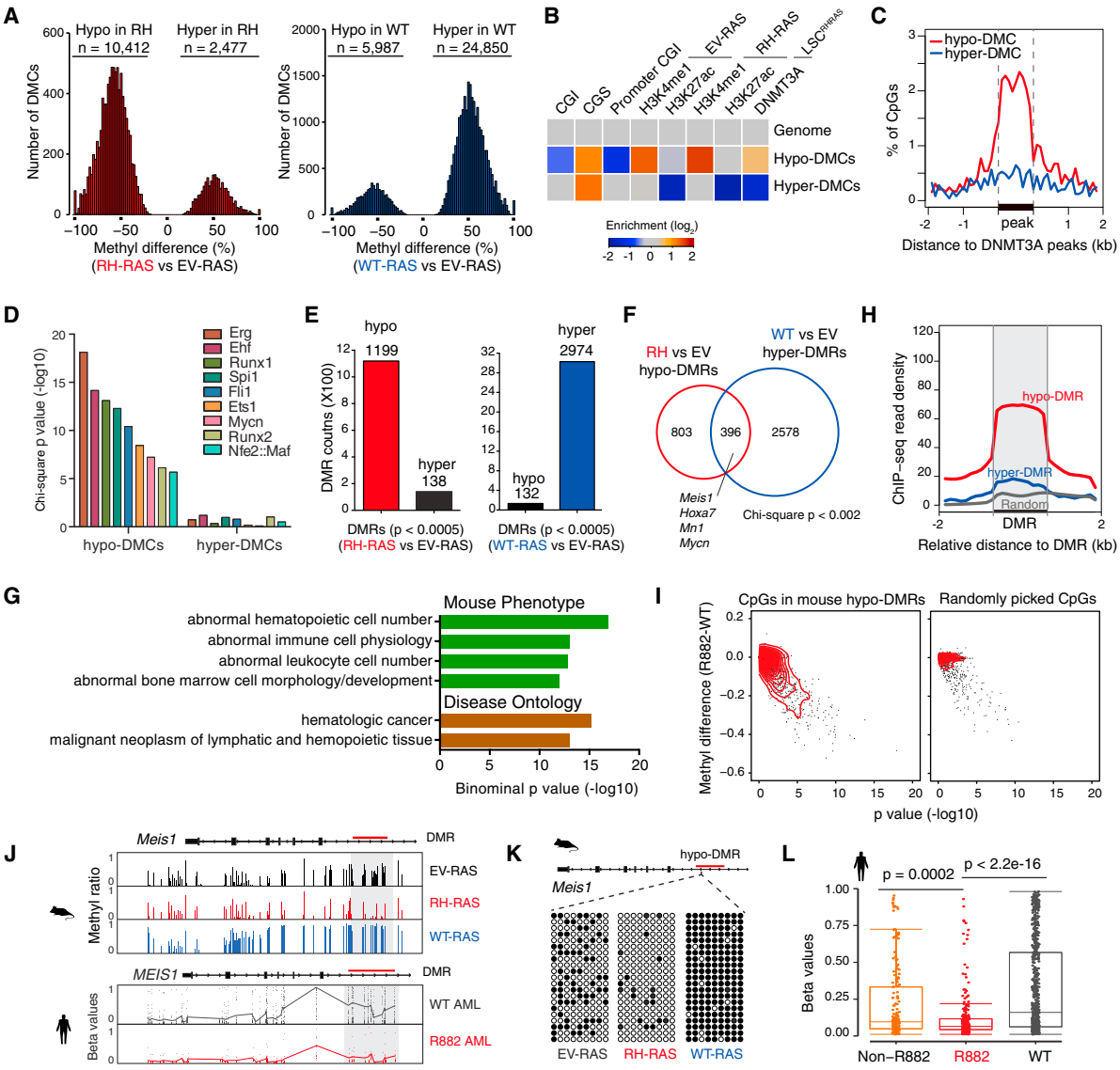

Figure 5. DNMT3A^{R882H} Induces Focal CpG Hypomethylations Enriched at H3K4me1-Demarcated, Gene-Regulatory Sites in HSPCs

(A) Distribution of DMCs (defined by q < 0.05) in the genome of murine HSPCs transduced with RH-RAS or WT-RAS, relative to EV-RAS.

(B) Heatmap showing enrichment of DNMT3A^{R882H}-associated DMCs at indicated genomic regions or ChIP-seq peaks in comparison with genome average. The enrichment value was calculated as $\log_2$(observed/expected) of the DMC numbers. CGI, CpG island; CGS, CpG shore.

(C) Distribution of DNMT3A^{R882H}-associated DMCs across DNMT3A^{R882H} ChIP-seq peaks (shown by a bold bar on x axis). y Axis shows percentage of DMCs located at 100-bp window of genomic regions centered on DNMT3A^{R882H} peaks.

(D) Enrichment of indicated TF binding motifs in DNMT3A^{R882H}-associated hypo-DMCs and hyper-DMCs.

(E) Summary of DMRs identified in the HSPCs with RH-RAS or WT-RAS, relative to EV-RAS.

(F) Venn diagram showing overlap of DNMT3A^{R882H} and DNMT3A^{WT}-associated DMRs.

(G) GREAT annotation of DNMT3A^{R882H}-associated hypo-DMRs.

(H) H3K4me1 profiles at DNMT3A^{R882H}-associated hypo-DMRs, hyper-DMRs, and random control regions. Plotted across DMRs (labeled by a bold line on x axis) were averaged H3K4me1 ChIP-seq read densities in EV-RAS cells.

(I) Scatterplots showing methylation changes of selected CpGs in human AMLs with DNMT3A R882 mutation relative to DNMT3A WT AMLs. Mean methylation differences (y axis) and p value (x axis) for each CpG between two AML patient groups were plotted. Left, CpGs in the human genome homologous to DNMT3A^{R882H}-associated hypo-DMRs identified in murine HSPCs; right, randomly picked CpG controls.

(J) DNA methylation profiles of Meis1 in indicated murine HSPCs and MEIS1 in human AMLs with WT (n = 50) or R882-mutated (n = 20) *DNMT3A*. Faded points show individual CpG methylation β values and connected lines indicate the mean methylation levels at each CpG site. Gray box and red bar represent a hypo-DMR in intron 6.

(K) Bisulfite sequencing of the Meis1 intron 6 DMR in indicated murine HSPC samples.

(legend continued on next page)

Because DNMT3A^{R882H}-induced hypo-DMRs can be found outside of gene-regulatory regions, we focused on those overlapping with a peak of H3K4me1 (a total of 777 DMRs) or H3K27ac (333 DMRs) in at least one cell condition and found that, in either case, 9- to 11-fold more DMRs showed enhanced H3K27ac levels than those with decreased H3K27ac (Figure 6F). These results indicate that DNA hypomethylation facilitates H3K27ac gain at gene-regulatory sites but also acts in a context-dependent manner. Consistently, more hypo-DMRs with gained H3K27ac were observed at regions showing a greater loss of CpG methylation (Figure 6G), supporting the degree of DNA hypomethylation as a contributing factor that fine-tunes functional output of gene-regulatory sites. Moreover, genes with increased H3K27ac at their hypo-DMRs were found to be enriched in HSPCs expressing RH-RAS relative to EV-RAS (Figure 6H), from which we identified 57 genes as both epigenetically altered and transcriptionally activated by DNMT3A^{R882H} (thus hereafter termed "DNMT3A^{R882H} signature genes," Figure 6I and Table S6). Notably, these DNMT3A^{R882H} signature genes included DNMT3A^{R882}-associated stemness genes studied above (a *Meis1-Mn1-Hoxa* node and *Mycn*) as well as other putative AML-promoting genes such as *Id2*, *Bcl2*, and *Runx3* (Figure 6I).

The *Meis1* Intron 6 Enhancer Carrying DNMT3A^{R882H}-Induced CpG Hypomethylation Is Crucial for *Meis1* Gene Activation in LSCs

To demonstrate a causal role of DNMT3A^{R882H}-induced focal DNA hypomethylation in gene-expression regulation, we cloned sequences from a panel of hypo-DMRs into a CpG-free reporter system designed to assess putative gene-regulatory activity and its relationship to CpG methylation (Schmidl et al., 2009). We found that all tested hypo-DMRs possess strong expression-enhancing activity in the absence of their CpG methylation (Figure 6J). CpG methylation of these hypo-DMRs completely abolished their expression-enhancing activities (Figure 6J), demonstrating a hypomethylation-dependent activation of *cis*-regulatory elements harbored within hypo-DMRs. To further verify DMR-associated enhancer activity in LSCs^{RH-RAS}, we closely examined a hypo-DMR located in the intron 6 of *Meis1* (Figure 6C, green bar) because *Meis1* is a critical effector gene for DNMT3A^{R882H}-associated AML progression (Figures 3H–3J) and this hypo-DMR is also found to be conserved in human AMLs with *DNMT3A* R882 mutation (Figures 5J–5L). Notably, this hypo-DMR is positive for H3K4me1 (Figure 6C) and has a significant overlap with a previously reported *MEIS1* enhancer in human cells (Xiang et al., 2014). First, we carried out chromosome conformation capture (3C), a surrogate assay for scoring enhancer usage and promoter association, and indeed detected a long-range looping interaction of the intron 6 hypo-DMR with the *Meis1* promoter in LSCs^{RH-RAS} (Figure 6K). To further determine the role of this putative intron 6 enhancer in DNMT3A^{R882H}-induced *Meis1* gene activation, we employed the CRISPR/Cas9-based genomic editing technology. Cas9 and a pair of single guide RNAs (sgRNA) targeting boundaries of the *Meis1* hypo-DMR were transduced into LSCs^{RH-RAS} (Figure 6L). PCR and direct sequencing confirmed sgRNA-mediated specific deletion of the hypo-DMR in five independent LSC^{RH-RAS} lines (Figures 6M, 6N, and S6N). In all cases, ablation of this putative enhancer significantly reduced *Meis1* expression (Figure 6O). Consistently, among human AMLs with *DNMT3A* R882 mutation, lower DNA methylation at the *MEIS1* intron 6 correlated with higher expression of *MEIS1* (Figure 6P). It is also worth noting that 54.5% (6 of 11) of *DNMT3A* WT AMLs display significant DNA methylation of *MEIS1* intron 6 and yet express *MEIS1* at high levels (Figure 6P), indicating that different gene activation mechanisms exist in these AML cases. Together, using *Meis1* as a paradigm example, we show that focal CpG hypomethylation induced by DNMT3A R882 mutation promotes enhancer activation and expression of key AML genes.

Dot1l Inactivation Suppresses DNMT3A^{R882H}-Associated LSC Properties and Aberrant Activation of Stemness Gene Programs

To explore the potential strategy for reversing DNMT3A^{R882H}-induced gene deregulation and thus treating *DNMT3A*-mutated leukemia, we conducted compound treatment studies with a collection of epigenetic regulator inhibitors and identified that LSCs^{RH-RAS} showed a significantly higher sensitivity to a Dot1l inhibitor, SGC0946, relative to control cells without *DNMT3A* mutation, i.e., LSCs expressing *NRAS^{G12D}* plus oncogenic TFs (Figure S7A). Dot1l, a histone H3 lysine 79 (H3K79) methyltransferase, belongs to a transcription elongation regulatory complex that engages acetylated histones at *cis*-regulatory sites (Li et al., 2014). Genomic profiling of H3K79 dimethylation (H3K79me2) detected its overall elevation at DNMT3A^{R882H}-associated hypo-DMRs in HSPCs (Figure 7A), as exemplified by those at *Meis1*, *Hoxa*, *Mn1*, and *Mycn* (Figures 7B and S7B). We confirmed H3K79me2 gain at these genes by ChIP-qPCR (Figure S7C). Next, we asked whether pharmacological inhibition of Dot1l could reverse DNMT3A^{R882H}-induced gene activation. We first confirmed SGC0946-mediated suppression of H3K79me2 in LSCs^{RH-RAS} (Figure S7D), followed by microarray profiling. Notably, after SGC0946 treatment, we detected significant downregulation of DNMT3A^{R882H} signature genes (Figures 7C and 7D) and concurrent upregulation of myeloid differentiation genes in LSCs^{RH-RAS} (Figures 7D and S7E). Although *Hoxa* and *Meis1* were shown as part of MLL-AF9 target genes that are dependent on Dot1l (Chen et al., 2015), the DNMT3A^{R882H} signature genes displayed a greater sensitivity to Dot1l inhibitors than MLL-AF9 targets in LSCs^{RH-RAS} (Figure 7E); conversely, the DNMT3A^{R882H} signature genes do not show overall response to Dot1l inhibitors in MLL-AF9-transformed AML cells (Figure S7F). These analyses indicate that *DNMT3A* R882 mutation confers a unique dependency on the Dot1l enzymatic activity in AML. We further verified downregulation of DNMT3A^{R882H}-associated

(L) Box plots of methylation β values of all CpGs (shown as dots in box plot) at MEIS1 intron 6 in human AMLs with R882-mutated DNMT3A (n = 20) relative to AMLs with either non-R882 mutated (n = 15) or WT (n = 50) DNMT3A. Horizontal line, median; box, interquartile range; whiskers extend to 1.5× the interquartile range. The p values were calculated by Mann-Whitney U test.
See also Figure S5; Tables S4 and S5.

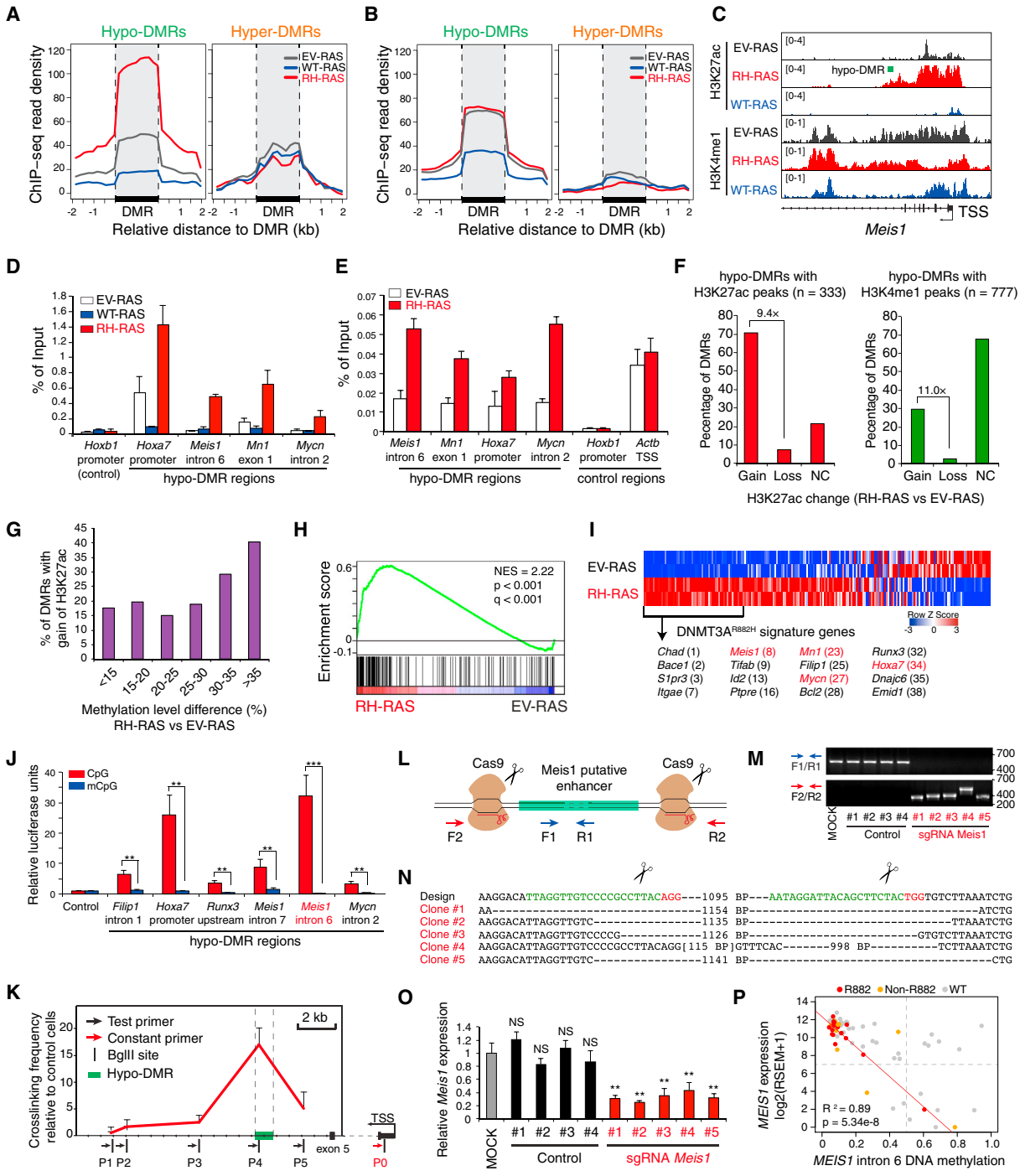

Figure 6. DNMT3A^{R882H}-Associated Hypo-DMRs Gain Epigenetic Alterations Associated with Gene Activation

(A and B) H3K27ac (A) and H3K4me1 (B) profiles at DNMT3A^{R882H}-associated DMRs (bold bar on x axis) and the surrounding regions. Averaged ChIP-seq read densities in HSPCs with EV-RAS, RH-RAS, or WT-RAS were plotted.

(C) H3K27ac and H3K4me1 profiles at *Meis1* intron 6 in indicated HSPCs. Green bar, hypo-DMR.

(D and E) ChIP-qPCR of H3K27ac (D) and p300 binding (E) at hypo-DMRs in indicated HSPCs.

(F) Percentage of DNMT3A^{R882H}-associated hypo-DMRs showing indicated H3K27ac changes in HSPCs with RH-RAS versus EV-RAS. Gain, increased H3K27ac; Loss, reduced H3K27ac; NC, no significant H3K27ac change. The total DMRs used for calculation were hypo-DMRs carrying H3K27ac (left) or H3K4me1 (right) in at least one cell condition.

(G) Percentage of DNMT3A^{R882H}-associated hypo-DMRs (n = 1,199) showing H3K27ac gain in HSPCs with RH-RAS versus EV-RAS, when these hypo-DMRs are divided based on degree of DNA methylation reduction (x axis) shown in the same samples.

(H) GSEA shows that genes with gain of H3K27ac at hypo-DMRs are enriched in HSPCs 16 days after transduction of RH-RAS, relative to EV-RAS.

(legend continued on next page)

stemness genes *Hoxa*, *Meis1*, *Mn1*, and *Mycn* after treatment with SGC0946 (Figures 7F, 7G, and S7G) or knockdown of Dot1l (Figures 7H, S7H, and S7I). In response to Dot1l inactivation, multiple murine and human AML lines bearing *DNMT3A* mutation showed suppressed in vitro growth (Figures 7I, S7J, and S7K) and concurrent cell differentiation (Figures 7J, 7K, and S7L–S7N). *DNMT3A*-mutated human AML lines also had decreased *HOXA* or *MEIS1* expression upon DOT1L blockade (Figures S7O and S7P). In contrast, various murine and human leukemia lines established by oncogenic TFs were all insensitive to Dot1l inhibition (Figures 7I and S7K). Also, enforced expression of HOXA9 plus MEIS1 reversed sensitivity of LSCs$^{RH\text{-}RAS}$ to Dot1l inhibition (Figure 7L), demonstrating a crucial role of these TFs in DNMT3A^{R882H}-mediated oncogenic effects. Importantly, knockdown of Dot1l in LSCs$^{RH\text{-}RAS}$ or their pretreatment with Dot1l inhibitors significantly delayed in vivo AML progression and prolonged the survival of engrafted mice (Figure 7M). Collectively, we show that expression of *DNMT3A*^{R882H} confers Dot1l dependency in AML and that reversing DNMT3A^{R882H}-induced gene activation by Dot1l inhibition may provide a potential therapeutic means for the treatment of AMLs with *DNMT3A* mutation.

DISCUSSION

In this study, we report a set of ex vivo LSC and in vivo murine AML model systems for studying the functionality of *DNMT3A* R882 mutation in AML pathogenesis. Using these human disease-mimicking models, we have (1) defined a causal role of DNMT3A^{R882H} in promoting AML transformation in vitro and in vivo; (2) identified DNMT3A^{R882H}-deregulated gene pathways, including a Meis1-Mn1-Hoxa TF node that we functionally validated as essential for DNMT3A^{R882H}-mediated AML progression; (3) shown that DNMT3A^{R882H} directly binds to gene-regulatory sites, notably enhancers, inducing focal DNA hypomethylation and concurrent gain of histone acetylation; (4) determined a critical role of the epigenetically altered enhancer and *cis*-regulatory elements for DNMT3A^{R882H}-associated gene activation; and (5) demonstrated, importantly, that pharmacological inhibition of Dot1l reverses the mutant DNMT3A-associated gene activation, thus providing a potential therapeutic avenue for the affected AMLs.

The molecular pathways identified in this study help explain several important biological phenomena related to *DNMT3A* mutation and hematological disease. First, as the Meis1-Mn1-Hoxa circuitry is crucial for both normal expansion of HSCs and malignant transformation of LSCs (Argiropoulos and Humphries, 2007; Heuser et al., 2011), deregulation of this TF node by R882-mutated DNMT3A provides a molecular explanation not only for malignant hematopoiesis but also for clonal hematopoiesis, a phenotype strongly associated with *DNMT3A* mutation (Genovese et al., 2014; Jaiswal et al., 2014; Xie et al., 2014). In addition, these findings help explain a mutually exclusive pattern for *DNMT3A* mutation and *MLL* rearrangement in AMLs (Cancer Genome Atlas Research Network, 2013; Patel et al., 2012) because the latter itself is a strong inducer of *Meis1* and *Hoxa* activation (Chi et al., 2010).

Our results also demonstrate the requirement of cooperation between *DNMT3A* mutation and the activated kinase such as RAS for AML induction. RAS mutation alone induces a hyperproliferative phenotype but does not support self-renewal, which is in agreement with previous studies (Zhang et al., 2009); RAS activation was also known to induce cell senescence, a barrier of cancer development (Campisi and d'Adda di Fagagna, 2007). On the other hand, *DNMT3A* mutation confers aberrant HSPC self-renewal, blocks differentiation programs, and yet lacks a pro-proliferation effect; besides a Meis1-Mn1-Hoxa node we have functionally confirmed as essential for DNMT3A^{R882H}-associated AML, other downstream targets of DNMT3A^{R882H}, such as pro-survival (*Bcl2*), anti-differentiation (*Id2*), and stemness (*Mycn*) genes, might be equally crucial for AML progression. These findings suggest that synergy between DNMT3A and kinase mutations is likely due to their differential effects on pathways relating to AML development. However, it is also possible that the two mutations may affect distinctive sets as well as the same sets of downstream effectors via genetic or epigenetic mechanisms. A similar synergy is most likely to exist between *DNMT3A* mutation and the activated FLT3, which acts upstream of RAS and coexists with the former in human AMLs as well.

Our studies clearly show that *DNMT3A* mutation-induced CpG hypomethylations are not random: they are significantly enriched at gene-regulatory sites, notably, putative enhancers marked by H3K4me1 as well as the binding sites of master hematopoietic TFs. Precise mechanisms by which CpG methylation of these *cis*-regulatory sites regulates gene expression remain to be fully studied. For example, despite a large number of DMCs found to be associated with either *DNMT3A* or *TET2* mutation in AML, a relatively small number of genes show changes in their expression (Russler-Germain et al., 2014; Shih et al., 2015). A possible

(I) Heatmap shows expression of genes in (H) ranked by higher expression in HSPCs with RH-RAS, relative to EV-RAS. The significantly upregulated genes in RH-RAS HSPCs are defined as "DNMT3A^{R882H} signature genes" (n = 57), with selected ones listed along with their respective rankings (bottom).

(J) Quantification of expression-enhancing activity of DNMT3A^{R882H}-associated hypo-DMRs with the embedded CpGs either non-methylated (CpG) or methylated (mCpG) using a CpG-free luciferase reporter system. The reporter without any DMR insertion was used as control. The p values were calculated by Student's t test.

(K) 3C assay shows looping interaction of the *Meis1* intron 6 hypo-DMR (P4) to gene promoter (P0), relative to other tested sites.

(L and M) Scheme (L) and PCR validation (M) of CRISPR/Cas9-mediated deletion of the *Meis1* intron 6 DMR. MOCK, parental LSC$^{RH\text{-}RAS}$; Control, no sgRNA; sgMeis1, a pair of sgRNAs that target the DMR boundaries.

(N) Sequencing of the genomic PCR products from F2/R2 primers shows CRISPR/Cas9-induced deletion of the *Meis1* intron 6 DMR.

(O) Expression levels of Meis1 in LSC$^{RH\text{-}RAS}$ lines shown in (M). The p values were calculated by Student's t test by comparing with MOCK.

(P) Impact of DNA methylation levels in *MEIS1* intron 6 in cytogenetically normal human AMLs grouped by *DNMT3A* WT (n = 45), non-R882 (n = 13), and R882 mutations (n = 16). Plotted were mean methylation β values of CpGs at *MEIS1* intron 6 and $\log_2$-transformed expression values of RNA sequencing by expectation maximization (RSEM). R^2 and p values shown were determined with data of R882-mutant AMLs.

Error bar denotes ±SD. **p < 0.01, ***p < 0.001; NS, not significant. See also Figure S6; Tables S4 and S6.

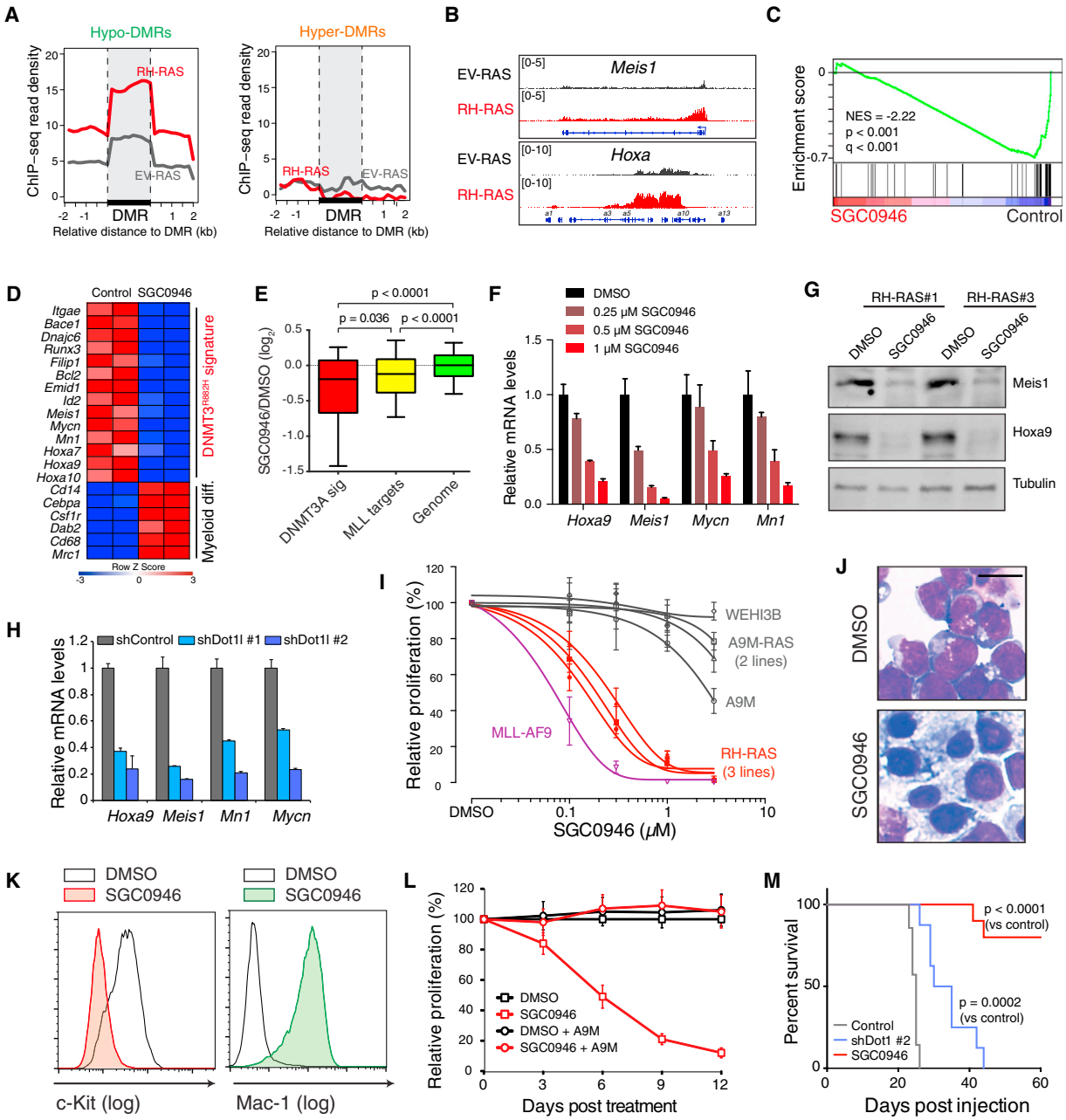

Figure 7. Dot1l Inhibition Reverses DNMT3A^{R882H}-Mediated Aberrant Transactivation of Stem Cell Genes, thereby Suppressing Acute Leukemogenicity

(A) Averaged H3K79me2 ChIP-seq signals at DNMT3A^{R882H}-associated hypo-DMRs and hyper-DMRs in HSPCs with RH-RAS or EV-RAS.

(B) H3K79me2 profiles at Meis1 and *Hoxa* in indicated HSPCs.

(C) GSEA shows downregulation of DNMT3A^{R882H} signature genes in LSCs^{RH-RAS} after treatment with 1 μM SGC0946 for 4 days.

(D) Heatmap shows downregulation of DNMT3A^{R882H} signature genes and upregulation of myeloid differentiation genes in SGC0946-treated LSCs^{RH-RAS} versus mock treatment.

(E) Box plots show relative expression of DNMT3A signature genes (n = 54), MLL-AF9 gene targets (n = 129), and all genes in the genome in SGC0946-treated LSCs^{RH-RAS}, relative to mock treatment. Horizontal line, median; box, interquartile range; whiskers, 10–90 percentiles. The p values were calculated by Mann-Whitney U test.

(F and G) qRT-PCR (F) and immunoblot (G) of indicated genes and proteins in LSCs^{RH-RAS} 6 days after treatment with SGC0946.

(H) Expression of indicated genes in LSCs^{RH-RAS} transduced with *Dot1l* shRNAs or vector control.

(I) Relative growth of LSCs^{RH-RAS} and other AML lines established by MLL-AF9, Hoxa9 plus Meis1 (A9M), A9M plus NRAS^{G12D} (A9M-RAS), and Hoxb8 plus Meis2 (WEHI3B) after a 12-day treatment with SGC0946 versus DMSO.

(J and K) Wright-Giemsa staining (J) and FACS analysis (K) of LSCs^{RH-RAS} 6 days after treatment with DMSO or 1 μM SGC0946. Scale bar, 10 μm.

(legend continued on next page)

explanation is that the effect of CpG methylation on gene expression is context dependent (Baubec and Schubeler, 2014): degree of CpG methylation change, density, or genomic location of CpG, methyl-CpG "readers," and TF binding are all possible factors affecting the ultimate effect of DNA methylation on gene expression. Unlike histone (de)acetylation, CpG (de) methylation at distal *cis*-regulatory sites such as enhancers may act as a permissive mechanism influencing gene expression, rather than a strong and instructive one controlling levels of gene activation and transcription. Nevertheless, using reporter assays and CRISPR/Cas9-mediated enhancer editing, we have determined the role of select hypo-DMRs in the activation of associated target genes such as *Meis1*.

This study also provides useful information on how to treat *DNMT3A*-mutated AMLs. Pharmacological blockade of Dot1l reversed *DNMT3A* mutation-induced gene activation, resulting in an impaired AML pathogenesis. In the future, examination of other "druggable" factors would likely identify additional therapeutic strategies for the treatment of *DNMT3A*-mutated AMLs. Therefore, in addition to elucidating the underlying oncogenic mechanisms, the ex vivo and in vivo model systems presented herein should be useful for exploring AML therapeutics.

EXPERIMENTAL PROCEDURES

The detailed procedures of plasmid construction, cell culture, antibody and immunoblot, flow cytometry, microarray analysis, ChIP-seq, eRRBS, Exome-seq, qRT-PCR, ChIP-qPCR, 3C-qPCR, shRNA-mediated knockdown, luciferase reporter assay, CRISPR/Cas9-mediated genomic editing, as well as the detailed information for computational and statistical analysis of deep sequencing data are described in Supplemental Experimental Procedures.

In Vitro CFU Assay with Serial Replating

Following lineage-negative (Lin^-) enrichment and retroviral transduction, 30,000 infected HSPCs were plated in the semi-solid methylcellulose cultivation system (Methocult; Stem Cell Technologies), followed by CFU counting and replating for every 10–14 days according to the manufacturer's protocol.

Animal Studies and In Vivo Leukemogenic Assay

All animal experiments were approved by and performed in accord with the guidelines of the Institutional Animal Care and Use Committee at the University of North Carolina. Leukemogenic potentials of transduced HSPCs were evaluated by bone marrow transplantation into sublethally irradiated syngeneic mice. In brief, 200,000 of bone marrow-derived Lin^- HSCPs following procedures of cytokine stimulation, retroviral transduction, and drug selection were injected via tail vein to recipient mice as described previously (Wang et al., 2009).

Statistical Analysis

Data are presented as the mean ± SD of three independent experiments unless otherwise noted. Statistical analysis was performed with Student's t test for comparing two sets of data with assumed normal distribution. We used a Mann-Whitney U test for data not showing a normal distribution, chi-square test for categorical variables, and log-rank test for Kaplan-Meier survival curves to determine statistical significance. $p < 0.05$ was considered significant.

ACCESSION NUMBERS

The microarray, eRRBS-seq, and ChIP-seq data reported in this paper have been deposited in the Gene Expression Omnibus with accession number GEO: GSE71475.

SUPPLEMENTAL INFORMATION

Supplemental Information includes Supplemental Experimental Procedures, seven figures, and six tables and can be found with this article online at http://dx.doi.org/10.1016/j.ccell.2016.05.008.

AUTHOR CONTRIBUTIONS

R.L. designed the research, performed experiments and computational analysis, interpreted data, and wrote the manuscript. P.W., S.R., and D.Z. performed computational analysis. T.P., Y.Z., and W.C. helped with animal modeling, viral transduction, and immunostaining studies, respectively. K.C. and P.A.W. participated in DNA methylome studies. O.A. helped with human AML cell studies. D.Z. supervised the computational studies. G.G.W. supervised the work, designed the research, interpreted data, and wrote the manuscript.

ACKNOWLEDGMENTS

We graciously thank Drs. Y. Xiong and K. Humphries for providing constructs, M. Kamps and M. Minden for leukemia lines, M. Torres for Meis1 antibody, D. Bauer and F. Zhang for CRISPR/Cas9 systems, M. Rehli for a CpG-free reporter, and J. Bear for an shRNA vector used in this study. Thanks to Drs. D. Allison and L. Cai and other members of the Wang laboratory for helpful discussion and technical support. We thank UNC's Genomics Core, Animal Studies Core, Flow Core, and HTSF core for their support of this work. This work is supported by NCI K99/R00 grant CA151683 to G.G.W., a DoD grant CA130247 to G.G.W., and grants of Gabrielle's Angel Foundation to O.A. and G.G.W. G.G.W. is an American Society of Hematology Scholar and a Kimmel Scholar. R.L. is a Lymphoma Research Foundation Postdoctorate Fellow. UNC Cores including the flow cytometry facility are supported in part by the North Carolina Biotech Center Institutional Support Grant 2012-IDG-1006 and UNC Cancer Center Core Support Grant P30 CA016086.

Received: July 21, 2015
Revised: March 3, 2016
Accepted: May 19, 2016
Published: June 23, 2016

REFERENCES

Abramovich, C., Pineault, N., Ohta, H., and Humphries, R.K. (2005). Hox genes: from leukemia to hematopoietic stem cell expansion. Ann. N. Y. Acad. Sci. *1044*, 109–116.

Argiropoulos, B., and Humphries, R.K. (2007). Hox genes in hematopoiesis and leukemogenesis. Oncogene *26*, 6766–6776.

Baubec, T., and Schubeler, D. (2014). Genomic patterns and context specific interpretation of DNA methylation. Curr. Opin. Genet. Dev. *25*, 85–92.

Bernt, K.M., Zhu, N., Sinha, A.U., Vempati, S., Faber, J., Krivtsov, A.V., Feng, Z., Punt, N., Daigle, A., Bullinger, L., et al. (2011). MLL-rearranged leukemia is dependent on aberrant H3K79 methylation by DOT1L. Cancer Cell *20*, 66–78.

Campisi, J., and d'Adda di Fagagna, F. (2007). Cellular senescence: when bad things happen to good cells. Nat. Rev. Mol. Cell Biol. *8*, 729–740.

(L) Effect of SGC0946 on growth of $LSCs^{RH\text{-}RAS}$ transduced with vector or Hoxa9 plus Meis1 (A9M). Relative proliferation was normalized to DMSO-treated cells. (M) Survival of mice engrafted with $LSCs^{RH\text{-}RAS}$, either mock-treated, stably transduced with a *Dot1l* shRNA, or pretreated with 1 μM SGC0946 ex vivo for 6 days. The p values were calculated by log-rank test.
Error bars denote ±SD. See also Figure S7 and Table S6.

Cancer Genome Atlas Research Network. (2013). Genomic and epigenomic landscapes of adult de novo acute myeloid leukemia. N. Engl. J. Med. *368*, 2059–2074.

Celik, H., Mallaney, C., Kothari, A., Ostrander, E.L., Eultgen, E., Martens, A., Miller, C.A., Hundal, J., Klco, J.M., and Challen, G.A. (2015). Enforced differentiation of Dnmt3a-null bone marrow leads to failure with c-Kit mutations driving leukemic transformation. Blood *125*, 619–628.

Challen, G.A., Sun, D., Jeong, M., Luo, M., Jelinek, J., Berg, J.S., Bock, C., Vasanthakumar, A., Gu, H., Xi, Y., et al. (2012). Dnmt3a is essential for hematopoietic stem cell differentiation. Nat. Genet. *44*, 23–31.

Chang, Y.I., You, X., Kong, G., Ranheim, E.A., Wang, J., Du, J., Liu, Y., Zhou, Y., Ryu, M.J., and Zhang, J. (2015). Loss of Dnmt3a and endogenous Kras(G12D/+) cooperate to regulate hematopoietic stem and progenitor cell functions in leukemogenesis. Leukemia *29*, 1847–1856.

Chen, C.W., Koche, R.P., Sinha, A.U., Deshpande, A.J., Zhu, N., Eng, R., Doench, J.G., Xu, H., Chu, S.H., Qi, J., et al. (2015). DOT1L inhibits SIRT1-mediated epigenetic silencing to maintain leukemic gene expression in MLL-rearranged leukemia. Nat. Med. *21*, 335–343.

Chi, P., Allis, C.D., and Wang, G.G. (2010). Covalent histone modifications—miswritten, misinterpreted and mis-erased in human cancers. Nat. Rev. Cancer *10*, 457–469.

Eppert, K., Takenaka, K., Lechman, E.R., Waldron, L., Nilsson, B., van Galen, P., Metzeler, K.H., Poeppl, A., Ling, V., Beyene, J., et al. (2011). Stem cell gene expression programs influence clinical outcome in human leukemia. Nat. Med. *17*, 1086–1093.

Genovese, G., Kahler, A.K., Handsaker, R.E., Lindberg, J., Rose, S.A., Bakhoum, S.F., Chambert, K., Mick, E., Neale, B.M., Fromer, M., et al. (2014). Clonal hematopoiesis and blood-cancer risk inferred from blood DNA sequence. N. Engl. J. Med. *371*, 2477–2487.

Guo, X., Wang, L., Li, J., Ding, Z., Xiao, J., Yin, X., He, S., Shi, P., Dong, L., Li, G., et al. (2015). Structural insight into autoinhibition and histone H3-induced activation of DNMT3A. Nature *517*, 640–644.

Heuser, M., Yun, H., Berg, T., Yung, E., Argiropoulos, B., Kuchenbauer, F., Park, G., Hamwi, I., Palmqvist, L., Lai, C.K., et al. (2011). Cell of origin in AML: susceptibility to MN1-induced transformation is regulated by the MEIS1/AbdB-like HOX protein complex. Cancer Cell *20*, 39–52.

Holz-Schietinger, C., Matje, D.M., and Reich, N.O. (2012). Mutations in DNA methyltransferase (DNMT3A) observed in acute myeloid leukemia patients disrupt processive methylation. J. Biol. Chem. *287*, 30941–30951.

Huang, Y., Sitwala, K., Bronstein, J., Sanders, D., Dandekar, M., Collins, C., Robertson, G., MacDonald, J., Cezard, T., Bilenky, M., et al. (2012). Identification and characterization of Hoxa9 binding sites in hematopoietic cells. Blood *119*, 388–398.

Jaiswal, S., Fontanillas, P., Flannick, J., Manning, A., Grauman, P.V., Mar, B.G., Lindsley, R.C., Mermel, C.H., Burtt, N., Chavez, A., et al. (2014). Age-related clonal hematopoiesis associated with adverse outcomes. N. Engl. J. Med. *371*, 2488–2498.

Jones, P.A. (2012). Functions of DNA methylation: islands, start sites, gene bodies and beyond. Nat. Rev. Genet. *13*, 484–492.

Kim, S.J., Zhao, H., Hardikar, S., Singh, A.K., Goodell, M.A., and Chen, T. (2013). A DNMT3A mutation common in AML exhibits dominant-negative effects in murine ES cells. Blood *122*, 4086–4089.

Krivtsov, A.V., Twomey, D., Feng, Z., Stubbs, M.C., Wang, Y., Faber, J., Levine, J.E., Wang, J., Hahn, W.C., Gilliland, D.G., et al. (2006). Transformation from committed progenitor to leukaemia stem cell initiated by MLL-AF9. Nature *442*, 818–822.

Lara-Astiaso, D., Weiner, A., Lorenzo-Vivas, E., Zaretsky, I., Jaitin, D.A., David, E., Keren-Shaul, H., Mildner, A., Winter, D., Jung, S., et al. (2014). Immunogenetics. Chromatin state dynamics during blood formation. Science *345*, 943–949.

Ley, T.J., Ding, L., Walter, M.J., McLellan, M.D., Lamprecht, T., Larson, D.E., Kandoth, C., Payton, J.E., Baty, J., Welch, J., et al. (2010). DNMT3A mutations in acute myeloid leukemia. N. Engl. J. Med. *363*, 2424–2433.

Li, Y., Wen, H., Xi, Y., Tanaka, K., Wang, H., Peng, D., Ren, Y., Jin, Q., Dent, S.Y., Li, W., et al. (2014). AF9 YEATS domain links histone acetylation to DOT1L-mediated H3K79 methylation. Cell *159*, 558–571.

Mayle, A., Yang, L., Rodriguez, B., Zhou, T., Chang, E., Curry, C.V., Challen, G.A., Li, W., Wheeler, D., Rebel, V.I., and Goodell, M.A. (2015). Dnmt3a loss predisposes murine hematopoietic stem cells to malignant transformation. Blood *125*, 629–638.

Noh, K.M., Wang, H., Kim, H.R., Wenderski, W., Fang, F., Li, C.H., Dewell, S., Hughes, S.H., Melnick, A.M., Patel, D.J., et al. (2015). Engineering of a histone-recognition domain in Dnmt3a alters the epigenetic landscape and phenotypic features of mouse ESCs. Mol. Cell *59*, 89–103.

Patel, J.P., Gonen, M., Figueroa, M.E., Fernandez, H., Sun, Z., Racevskis, J., Van Vlierberghe, P., Dolgalev, I., Thomas, S., Aminova, O., et al. (2012). Prognostic relevance of integrated genetic profiling in acute myeloid leukemia. N. Engl. J. Med. *366*, 1079–1089.

Rada-Iglesias, A., Bajpai, R., Swigut, T., Brugmann, S.A., Flynn, R.A., and Wysocka, J. (2011). A unique chromatin signature uncovers early developmental enhancers in humans. Nature *470*, 279–283.

Russler-Germain, D.A., Spencer, D.H., Young, M.A., Lamprecht, T.L., Miller, C.A., Fulton, R., Meyer, M.R., Erdmann-Gilmore, P., Townsend, R.R., Wilson, R.K., and Ley, T.J. (2014). The R882H DNMT3A mutation associated with AML dominantly inhibits wild-type DNMT3A by blocking its ability to form active tetramers. Cancer Cell *25*, 442–454.

Schmidl, C., Klug, M., Boeld, T.J., Andreesen, R., Hoffmann, P., Edinger, M., and Rehli, M. (2009). Lineage-specific DNA methylation in T cells correlates with histone methylation and enhancer activity. Genome Res. *19*, 1165–1174.

Schubeler, D. (2015). Function and information content of DNA methylation. Nature *517*, 321–326.

Shih, A.H., Abdel-Wahab, O., Patel, J.P., and Levine, R.L. (2012). The role of mutations in epigenetic regulators in myeloid malignancies. Nat. Rev. Cancer *12*, 599–612.

Shih, A.H., Jiang, Y., Meydan, C., Shank, K., Pandey, S., Barreyro, L., Antony-Debre, I., Viale, A., Socci, N., Sun, Y., et al. (2015). Mutational cooperativity linked to combinatorial epigenetic gain of function in acute myeloid leukemia. Cancer Cell *27*, 502–515.

Shlush, L.I., Zandi, S., Mitchell, A., Chen, W.C., Brandwein, J.M., Gupta, V., Kennedy, J.A., Schimmer, A.D., Schuh, A.C., Yee, K.W., et al. (2014). Identification of pre-leukaemic haematopoietic stem cells in acute leukaemia. Nature *506*, 328–333.

Wang, G.G., Pasillas, M.P., and Kamps, M.P. (2005). Meis1 programs transcription of FLT3 and cancer stem cell character, using a mechanism that requires interaction with Pbx and a novel function of the Meis1 C-terminus. Blood *106*, 254–264.

Wang, G.G., Pasillas, M.P., and Kamps, M.P. (2006). Persistent transactivation by meis1 replaces hox function in myeloid leukemogenesis models: evidence for co-occupancy of meis1-pbx and hox-pbx complexes on promoters of leukemia-associated genes. Mol. Cell Biol. *26*, 3902–3916.

Wang, G.G., Cai, L., Pasillas, M.P., and Kamps, M.P. (2007). NUP98-NSD1 links H3K36 methylation to Hox-A gene activation and leukaemogenesis. Nat. Cell Biol. *9*, 804–812.

Wang, G.G., Song, J., Wang, Z., Dormann, H.L., Casadio, F., Li, H., Luo, J.L., Patel, D.J., and Allis, C.D. (2009). Haematopoietic malignancies caused by dysregulation of a chromatin-binding PHD finger. Nature *459*, 847–851.

Wong, P., Iwasaki, M., Somervaille, T.C., So, C.W., and Cleary, M.L. (2007). Meis1 is an essential and rate-limiting regulator of MLL leukemia stem cell potential. Genes Dev. *21*, 2762–2774.

Xiang, P., Wei, W., Lo, C., Rosten, P., Hou, J., Hoodless, P.A., Bilenky, M., Bonifer, C., Cockerill, P.N., Kirkpatrick, A., et al. (2014). Delineating MEIS1 cis-regulatory elements active in hematopoietic cells. Leukemia *28*, 433–436.

Xie, M., Lu, C., Wang, J., McLellan, M.D., Johnson, K.J., Wendl, M.C., McMichael, J.F., Schmidt, H.K., Yellapantula, V., Miller, C.A., et al. (2014).

Age-related mutations associated with clonal hematopoietic expansion and malignancies. Nat. Med. *20*, 1472–1478.

Xu, J., Wang, Y.Y., Dai, Y.J., Zhang, W., Zhang, W.N., Xiong, S.M., Gu, Z.H., Wang, K.K., Zeng, R., Chen, Z., and Chen, S.J. (2014). DNMT3A Arg882 mutation drives chronic myelomonocytic leukemia through disturbing gene expression/DNA methylation in hematopoietic cells. Proc. Natl. Acad. Sci. USA *111*, 2620–2625.

Yan, X.J., Xu, J., Gu, Z.H., Pan, C.M., Lu, G., Shen, Y., Shi, J.Y., Zhu, Y.M., Tang, L., Zhang, X.W., et al. (2011). Exome sequencing identifies somatic mutations of DNA methyltransferase gene DNMT3A in acute monocytic leukemia. Nat. Genet. *43*, 309–315.

Yang, L., Rau, R., and Goodell, M.A. (2015). DNMT3A in haematological malignancies. Nat. Rev. Cancer *15*, 152–165.

Zhang, J., Wang, J., Liu, Y., Sidik, H., Young, K.H., Lodish, H.F., and Fleming, M.D. (2009). Oncogenic Kras-induced leukemogeneis: hematopoietic stem cells as the initial target and lineage-specific progenitors as the potential targets for final leukemic transformation. Blood *113*, 1304–1314.